



Surficial sediment remobilization by shear between sediment and water above tsunamigenic megathrust ruptures: experimental study

Chloé Seibert¹, Cecilia McHugh^{2,1}, Chris Paola³, Leonardo Seeber¹, James Tucker³

¹Lamont-Doherty Earth Observatory of Columbia University, Palisades New York, USA

5 ²Queens College, City University of New York, School of earth and Environmental Sciences, New York 11367, USA

³Department of Earth and Environmental Sciences, St Anthony Falls Laboratory, University of Minnesota, Minneapolis, MN, USA

Correspondence to: Chloé Seibert (cseibert@ldeo.columbia.edu)

Abstract. Large megathrust earthquakes that rupture the shallow part of the interface can cause unusually large co-seismic
10 displacements and tsunamis. The long duration of the seismic source and high upper-plate compliance contribute to large and
protracted long-period motions. The resulting shear stress at the sediment/water interface in, for example, the Mw9.0 2011
Tohoku-Oki earthquake, could account for the surficial sediment remobilization identified on the outer margin. Through
physical tank experiments, we test this hypothesis by exploring shear between sediment and water, interactions between high
and low frequency seismic waves, and sediment properties (chemistry, grain size, water content and salinity). Our results show
15 that low-frequency motion during a 2011-like earthquake can entrain several centimeters of surficial sediment and that
entrainment can be enhanced by high-frequency vertical oscillations. These experiments validate a new mechanism of co-
seismic sediment entrainment in deep-water environments.

1 Introduction

All earthquakes in the $\geq M9.0$ class originate from subduction megathrusts boundaries. Despite their high tsunamigenic risk,
20 such earthquakes are still poorly understood, as demonstrated by the last two earthquakes in this class, the Mw9.3 2004
Sumatra-Andaman and the Mw9.0 2011 Tohoku-Oki events (Lay, 2015). They ruptured the shallowest portion of the
megathrust, which had been considered aseismic and was responsible for their catastrophic tsunamis. Five events of this size
have been experienced in the last century, but the lack of data about them leads to two critical needs for constraining global
hazard: 1) identifying subduction boundaries capable of producing very large earthquakes; and 2) determining the recurrence
25 of these events.

Characterization of earthquake event deposits in the offshore sedimentary record has extended earthquake catalogs into pre-
history and improved seismic hazard estimations (e.g. Goldfinger et al., 2003, 2012; Pouderoux et al., 2014; Ratzov, et al.,
2015; Usami et al., 2018; Seibert et al., 2024). Current work aims to relate distinctions among event deposits with earthquake



characteristics such as magnitude and source locations (Goldfinger et al., 2013; Moernaut et al., 2017; Van Daele et al., 2019; McHugh et al., 2020; Howarth et al., 2021).

Understanding event deposits starts with sediment entrainment. The premise in sediment dynamics has been that the bed is fixed, and the fluid moves relative to it, creating shear stress that entrains sediment. Seafloor motion from large subduction earthquakes can be so large that alone could move the bed relative to ambient water fast enough to entrain sediment (Gomberg, 2018). The implication for paleoseismology is that large megathrust earthquakes could mobilize sediment in places where that would otherwise be unlikely, creating distinctive sedimentary signatures.

As one of the most instrumented in history, the Tohoku-Oki earthquake and tsunami provided detailed ground-truths to relate with specific sedimentary signatures, including: a persistent deep sediment suspension (Noguchi et al., 2012; Oguri et al., 2013); a tsunami-remobilized sediment possibly sourcing turbidity currents to the upper slope (Arai et al., 2013; Toyofuku et al., 2014; Tamura et al., 2015; Usami et al., 2017); large slumps at the trench (Kodaira et al., 2012; Strasser et al., 2013); turbidity flows originating on the slope and trench (Ikehara et al., 2014, 2016; Molenaar et al., 2019); and surficial sediment remobilization over ~100's of km² including the mid-slope terrace and trench (McHugh et al., 2016, 2020). McHugh et al. (2016) documented this mechanism using short-lived radioisotopes. They highlighted 2011 event deposits consisting of a basal turbidite overlain by a homogeneous muddy flow deposit (from 3 to 200 cm-thick). These mud layers are enriched in excess (xs)²¹⁰Pb that has not decayed and is in steady state, requiring a source from the upper few cm of sediment. This source must also be widespread, to account for the thickness of the deposits. In addition to the Japan Subduction zone, surficial sediment remobilization has been documented along the Nankai accretionary prism (Ashi et al., 2014) and in Chilean lakes (Moernaut et al., 2017; Molenaar et al., 2021).

In this paper, we focus on surficial entrainment described in Japan (McHugh et al., 2016, 2020) and on large-amplitude long-period seismic motion on the outer upper plate as a possible cause. The spectrum of seismic waves broadens toward long periods for larger earthquakes, particularly for ones that include the slow-rupturing shallowest part of the megathrust (e.g. Lay, 2015). This suggests that retrieving a fingerprint of long-period seismic motion in sediment records may open opportunities to differentiate the sedimentary signatures of the largest earthquakes.

From published results about the 2011 M9.0 rupture, we estimate the co-seismic long-period motions on the Japan slope-trench margin, and we report on laboratory experiments testing their potential for entraining sediments. We believe these are the first experiments on entrainment that combine high-frequency shaking of the sediment with shear between sediment and water that captures the effects of long period motions. We also provide initial observations on how sediment properties (grain size, mineralogy, water content and salinity) affect surficial sediment remobilization.

2 Conceptual model

The Tohoku-Oki earthquake ruptured the entire brittle depth range of the Japan erosional subduction boundary. From its nucleation, this rupture propagated both down dip into the mantle and up-dip to the trench (Fig. 1A). The co-seismic



displacement increased up-dip, reaching ~60 m at the trench (Lay et al., 2011a; Fujiwara et al., 2011). Based on observations in Japan and elsewhere, Lay et al. (2012) subdivided the subduction interface in depth domains that radiate seismically with distinct spectral characteristics (Fig. 1A). In the shallowest of these megathrust domains, the rupture radiates preferentially at low frequencies (Lay et al., 2011b). This rupture domain underlies the outer part of the margin, where low rigidity (Fig. 1) and low seismic velocities (Kodaira et al., 2017) independently characterize the upper plate. Seismic attenuation is proportional to frequency and in the outer upper plate it is likely to be high due to the presence of fluids rising from the subduction channel (e.g. Escobar et al., 2019), contributing further to a spectral shift toward the long period at the sea floor. An important contribution to long-period oscillations of the seafloor, however, may come from the resonance coupling between a horizontally polarized fundamental shear mode of oscillation of the outer upper-plate wedge and the oceanward displacement of this wedge during rupture (Fig. 1A).

In an area ~50 km wide from the trench on the upper plate (Fig. 1B) and ~100 km along it, the static horizontal displacements at the seafloor (Fujiwara et al., 2011) and at the megathrust (Yue & Lay, 2011, 2013) are both about ~50 m. Low rigidity and possible inelastic relaxation of the upper plate (G. Ekstrom personal communication) may account for the lack of attenuation and large size of the displacement. In addition, the first motion includes a dynamic component that can be as much as 30% of the static displacement (e.g. Yue & Lay, 2011, Fig. 1A). Thus, the initial eastward displacement of the seafloor at the outer margin could have been ~65 m. This seafloor motion is primarily driven by the displacement on the patch of the megathrust below it. This displacement is accomplished in about ~40 seconds and the rupture propagates across the area in our Figure 1B in ~20 seconds (Yue & Lay, 2011). Thus ~1 m/s is a reasonable estimate of the average velocity of the seafloor above the outer wedge during its ~60 seconds first pulse of eastward displacement. This pulse includes the static displacement and a dynamic overshoot, which is the first cycle of the reverberation that follows. The rupture displacement is expected to drive the upper plate eastward and upward. Assuming that the water column above it moves only upward (e.g. Fujiwara et al., 2011), the relative motion between water and the uppermost sediment should be nearly equal to the motion of the seafloor on the upper plate, producing shear velocities ~1 m/s during the ~1 minute of the first motion. This duration may be extended if peak velocities in the early oscillations can reach similar velocities to the first one (Fig. 1B).

Based on available seismic velocities (Kodaira et al., 2017), we calculate the fundamental periods of horizontally polarized shear waves with nodes at the top of the subducting slab and “crests” at the seafloor (Fig. 1B and S1). These periods tend to increase landward as the upper plate thickens but remain close to ~10 s over a ~30 km wide belt of the outer margin centered on the mid-slope terrace (Fig. 1B). Amplitude and duration enhancements of seismic waves in narrow frequency bands are typical of sedimentary basins, but they have recently been also recognized at active margins by in-situ deep-water measurements of long-period teleseismic waves (Nakamura et al., 2015; Gomberg, 2018). Lower seismic velocities at outer active margins are usually ascribed to accretion of water-rich sediment and tectonic deformation (e.g. Kodaira et al., 2020). The main purpose of this work is to test whether such long-period motion can develop sufficient water-sediment differential velocity and shear stress to entrain the surficial sediment, and whether high-frequency vertical acceleration can enhance this entrainment (Gomberg, 2018).

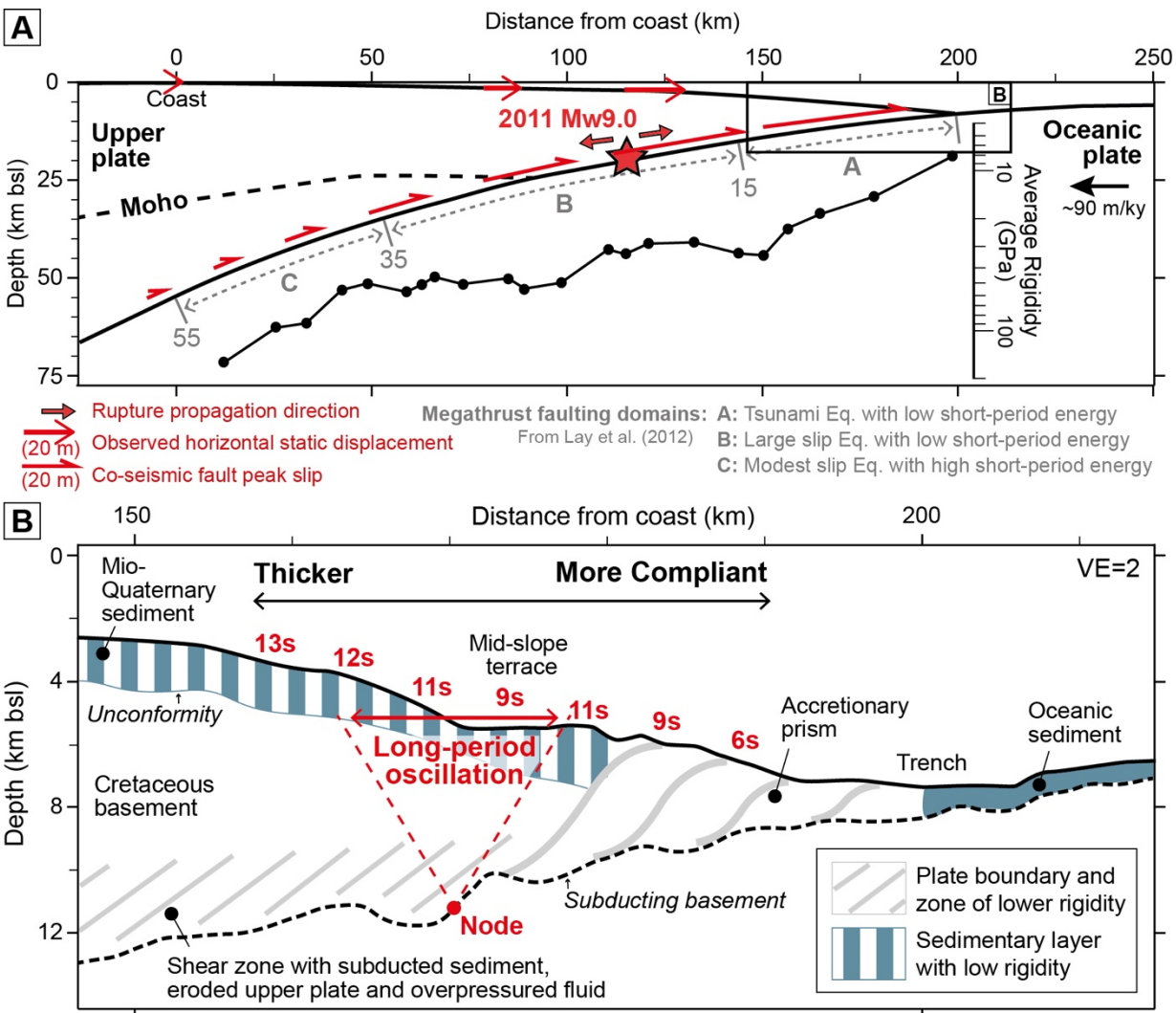


Figure 1: Profile across the Japan active margin at the 2011 Mw9.0 Tohoku-Oki megathrust rupture. A. Schematic cross section showing hypocenter and rupture initiation (red start) and megathrust domains A, B and C modified from Lay et al. (2012) (no vertical exaggeration). Mean values of rigidity in depth bins from seismic-rupture radiation averaged for a number of megathrusts (Lay and Bilek, 2007). Note order of magnitude increase across the seismogenic range. Red half-arrows show peak co-seismic slip from Lay et al. (2012). Red arrows show the horizontal static displacement from Yue and Lay (2013). B. The outer upper plate above the largest 2011 rupture displacements (based on MCS profile D11). Periods of fundamental-mode horizontally polarized oscillation (red) (Fig. S1). The landward increases in wedge thickness and S-wave velocity (i.e., rigidity; Von Huene et al., 1994; Fujiwara et al., 2011) allow for a ~20km wide plateau in fundamental periods at ~10 sec centered on the Mid-Slope Terrace.

3 Physical experiment setup

Earthquake Motion. Our experiments (Text S1) simplify the full spectrum of earthquake motion into two essential components: 1) quasi-steady shear at the sediment-water interface produced by the static displacement and ensuing oscillations of the outer upper plate, which is simulated by steady flow of water over sediment; and 2) high-frequency P-waves (1-10 Hz), which are simulated by vertical shaking of water and sediment within a rectangular duct (Fig. 2a and 2b).

Sediment and water Composition. Mixtures of fine sand, silt and clay-size bentonite simulated sediments. The first series of experiments used two sediment mixtures characterized by a low (10%) and high (40%) fine sand content, with the remainder composed equally of silt and clay, labelled Mix#1 and Mix#2, respectively (Table S1). We investigated the role of water with freshwater content ranging from 50 to 80% by weight (implying 50 to 20% of sediment content in the mixture, respectively). We also did runs with Mix#3, which had the same dry sediment as Mix#2, but with saline rather than fresh water (Table S1).

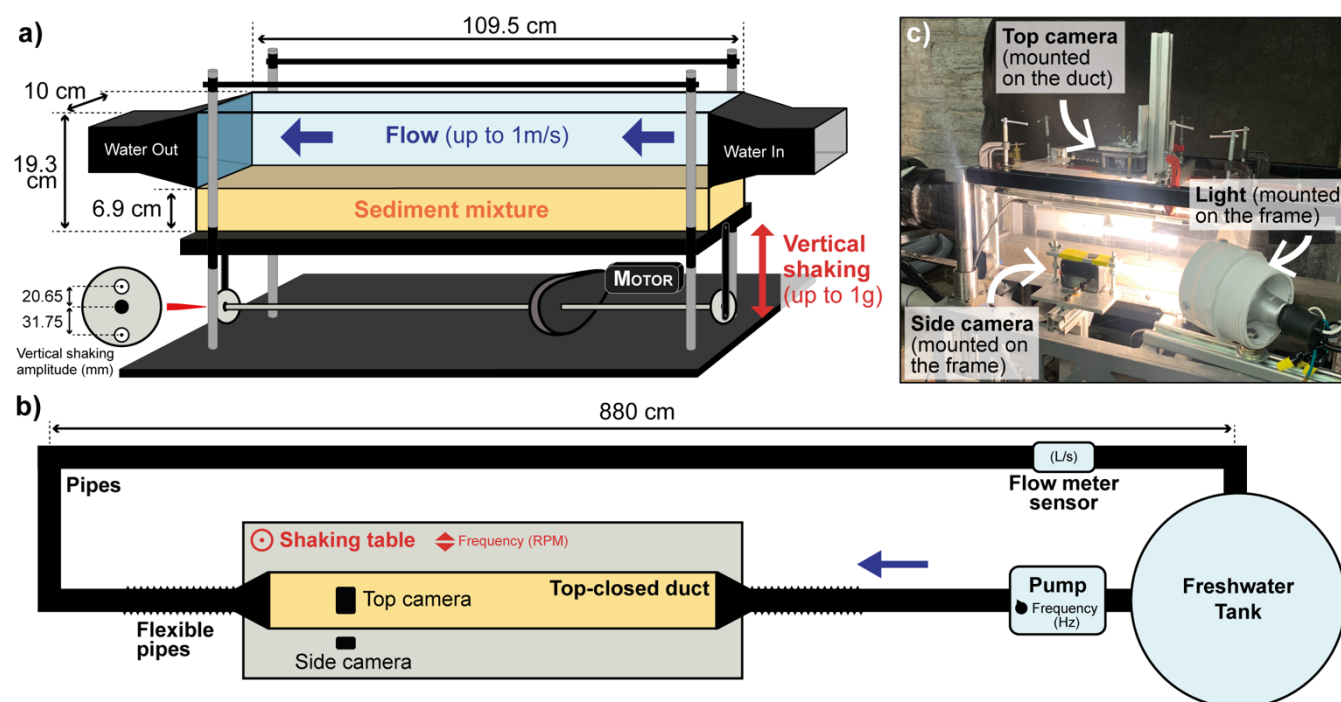


Figure 2: Physical experiment set up. a) Details of the duct with sediment and water. The shaking table amplitudes are set 20.65 mm or 31.75 mm for each run. b) Top view of the system. c) Photo of the downstream duct area targeted for data recording.

4 Physical experiment results

The first set of experiments compared erosion rates caused by flow in different settings. Mean flow velocity U and vertical peak acceleration a_v were constant in each run, but varied among the runs: 0-1 m/s and 0 or 1g respectively (Fig. 3). We calculated erosion rates r_v in two ways: 1) by differencing bed topography before and after the run; and 2) by measuring from videos from one side of the duct. Both methods provide consistent results (Table S2). We identified two processes of bed erosion: 1) grain-by-grain erosion; and 2) stripping, characterized by a sudden entrainment of a cm-thick layer of sediment. Once entrained by either mechanism, the sediment is transported out of the duct as bedload and/or suspension.

For sediment Mix#1 and $U = 1$ m/s flow velocity, erosion rates are low, ~ 0.03 cm/min, with grain-by-grain entrainment, regardless of water content and a_v (Fig. 3). Vertical shaking has no clear effect on entrainment rate even at $a_v = 1$ g. Results for Mix#2 depend on water content. With 50% and 60% water content and $U = 1$ m/s, r_v ranges from 0.008 to 0.029 cm/min with predominantly grain-by-grain entrainment. With 70 % freshwater and $U = 0.8$ m/s, we observe two phases (Fig. S2): the first minutes show grain-by-grain entrainment and $r_v = 0.08 - 0.18$ cm/min, Table S2); then the upper part of the bed is stripped, greatly increasing r_v (1.3 and 1.5 cm/min, Fig. 3 and Table S2). With a flow velocity of 1 m/s, the entire bed is eroded by stripping in 90 s. With 80% water content, r_v for Mix#2 increases to 0.7 - 0.9 cm/min with $U = 0.5$ m/s (Fig. 3). There is no major stripping but sediment waves developed at the bed interface. With sea water in the mixture (Mix#3), r_v increases dramatically, to 3 cm/min, even with $U = 0.5$ m/s (Fig. 3). Finally, for the same mixture and flow velocity, erosion rates are higher when the sediment is subjected to $a_v = 1$ g (runs with 70 % and 80 % water on Fig. 3, Table S2).

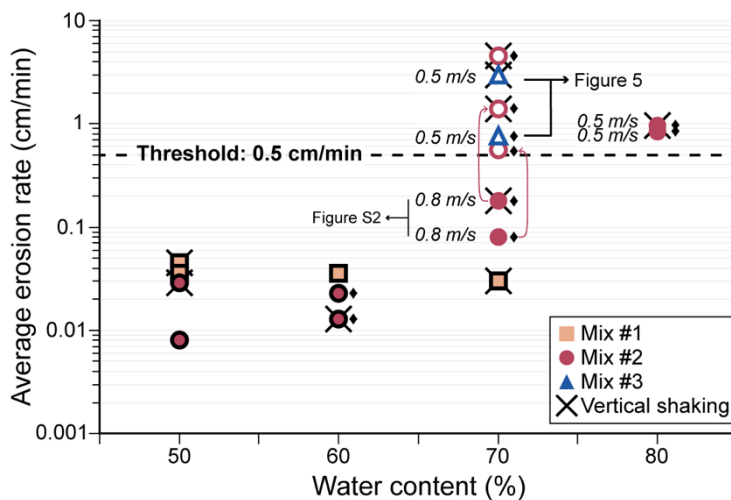


Figure 3: Entrainment versus sediment water content. Entrainment involves single grains only (full symbol), includes clumps of sediment (black diamonds), as above, but with major rapid stripping (empty symbol). Each dot highlights the mean erosion rate over a run, but arrows link distinct erosion steps in the same run (the symbols at the start of the arrow show the mean erosion rate of the first step and the symbols at the end of the arrow show the mean erosion rate considering both steps). The crosses mark runs with a fixed vertical shaking at 3.5 Hz (with an amplitude of 20.65 mm) and an acceleration of 1 g. No shaking in other runs. The flow velocity was set up at a constant 1 m/s, unless specified. While the black outline indicates that the run lasted 10 min, the other runs were shorter due to the high erosion rates.



The compared erosion rate versus flow velocity for each of the three mixtures with 70% water content is shown on Figure 4. The runs have no vertical shaking, and a gradual increase of the flow velocity. Values of r_v for Mix#1 and Mix#2 remain low (< 0.1 cm/min) but show distinct trends (Fig. 4A). With Mix#1, erosion starts with $U = 0.35$ m/s and increases up to 0.02 cm/min at about 0.6 m/s, but then remains constant for velocities from 0.6 to 1.0 m/s. With Mix#2, erosion starts with a $U = 0.3$ m/s and increases up to 0.08 cm/min at 0.8 m/s. Figure 4B highlights the significant impact of salinity on entrainment. Erosion rates at $U = 0.5$ m/s are 100 times higher for Mix#3 than for Mix#1 and Mix#2.

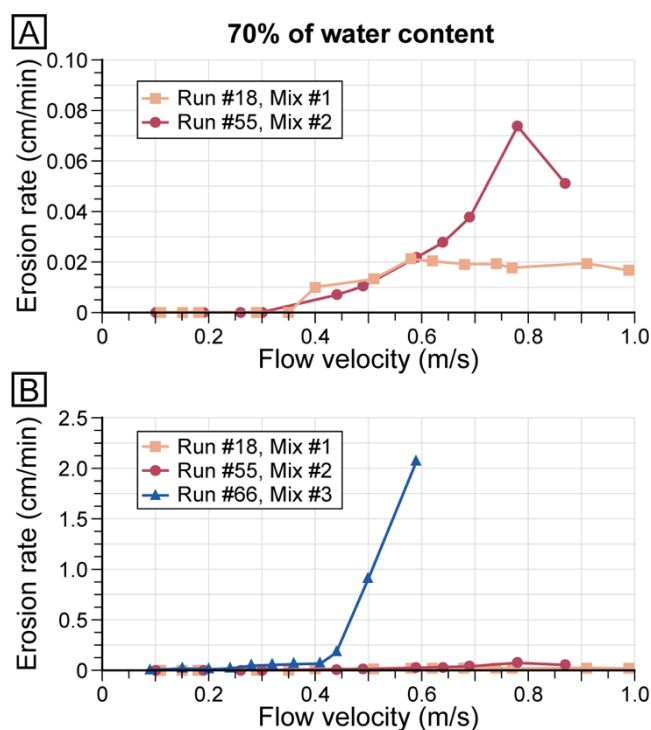


Figure 4: Evolution of the erosion rate for 3 representative runs (one for each mixture with a water content of 70 %) with no vertical shaking and increasing the flow gradually. The plots A and B show the same curves for the Mix#1 and #2, but with an expanded vertical scale for the Mix#3 run.

A closer look at the evolution of erosion rates over time for the Mix#3 runs shows the same trend with or without vertical shaking. During the first seconds, the sediment is eroded by stripping, leading to a_v values up to 13 cm/min and 10.5 cm/min for runs 67 and 69, respectively (Fig. 5). In a second phase, the erosion occurs grain-by-grain and via sediment clumps, with strong influence by the vertical shaking. With $a_v = 0$, r_v ranges between 0.2 and 0.9 cm/min (Run 67, Fig. 5) and between 1.8 and 2.9 cm/min for $a_v = 1g$ (Run 69, Fig. 5).

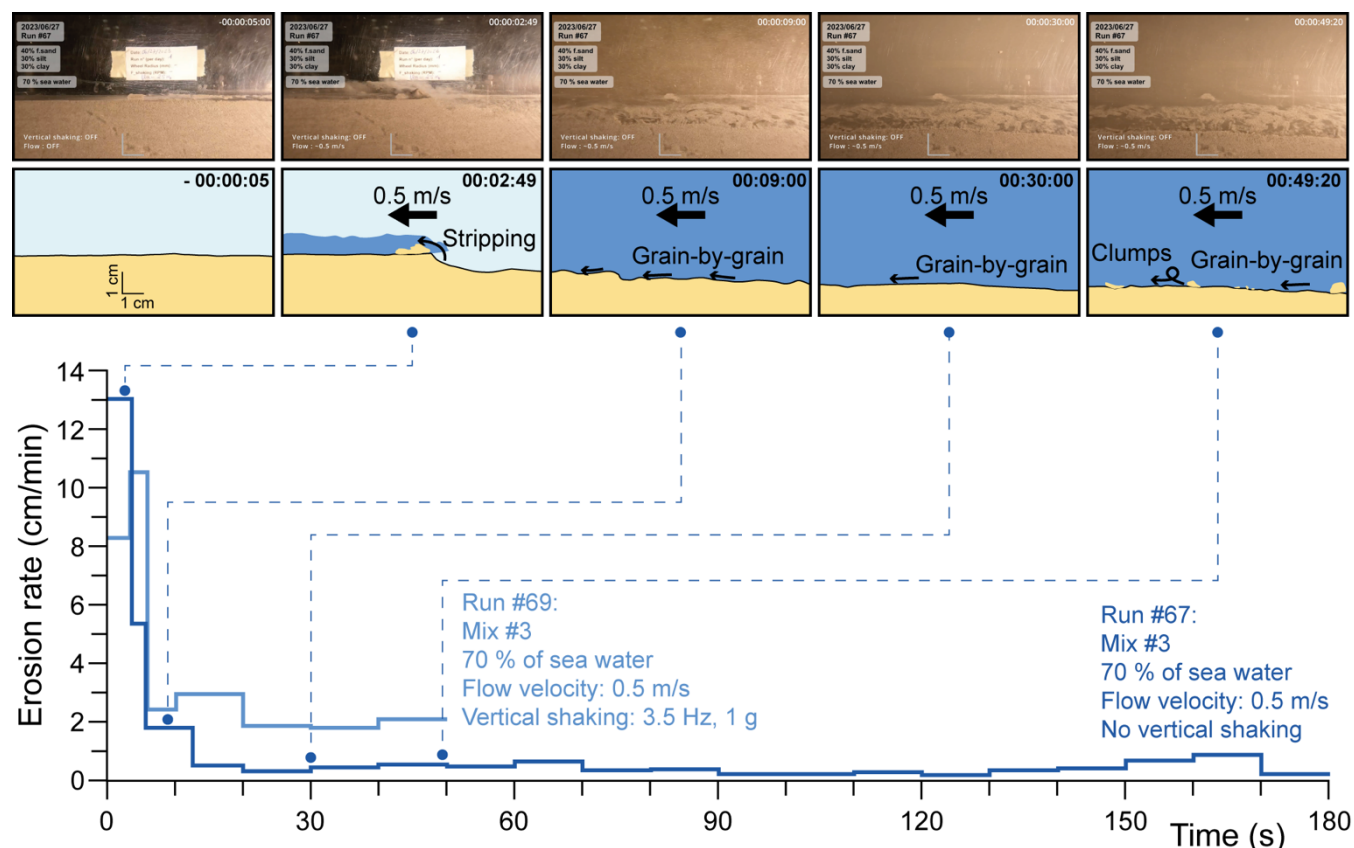


Figure 5: Evolution of the erosion rate of Mix#3 sediment. The erosion rates are calculated over 10 s-intervals but more often for the first ~10 seconds of each run. The photos and their interpretative cartoons highlight different steps of run #67.

5 Discussion and Conclusion

The initial experimental results we report here show that the seafloor motion of the outer upper plate in response to the 2011 M9.0 rupture could cause widespread entrainment of surficial sediment with grain sizes and water contents consistent with the abyssal floor. Generally, our laboratory studies distinguish modes of remobilization that result from the interplay of high-frequency and low-frequency motions. They show that relative shear between the seabed and water column compatible with a large rupture can effectively entrain surficial sediment and lead to the types of event deposits created by the Tohoku-Oki earthquake. The short-lived radioisotopes measured from the submarine deposits demonstrated that the Tohoku-Oki earthquake triggered remobilization of the upper few centimeters of sediment over a wide area of the seafloor (McHugh et al., 2016). Based on this thickness and considering a duration of several minutes for the strong motion, including rupture and reverberation (Nakamura et al., 2015; Gomborg, 2018), we propose a threshold a_v value of ~0.5 cm/min, above which the erosion rate of surficial sediment is consistent with the field data (Fig. 3).



Our investigation of the surficial sediment entrainment under controlled conditions highlights that the intensity of the seismic waves is not the only factor. The composition and the physical properties (e.g. water content, shear strength) of the sediment also strongly influence its susceptibility to entrainment. The results obtained with Mix#2, enriched in sand-size particles, show the impact of the water content on entrainment. Entrainment by stripping occurs in Mix#2 with $\geq 70\%$ water, whereas erosion is insignificant below it (Fig. 3). In the field, the water content of the sediment decreases with increasing sediment burial due to compaction, typically reaching about 50% at a depth of 10 - 20 cm. Thus, entrainment of surficial sediment by long-period motion is likely to be limited by the depth to more compacted sediment. Clay concentration and the ionic strength of the interstitial water (freshwater or sea water) are also significant factors (Fig. 4). Other parameters that could affect sediment entrainment include components like diatoms, ashes, organic matter biofilms, and also the nature and intensity of bioturbation. The long-period motions (i.e. the quasi-steady flow in our experiments) can effectively remobilize relatively weak sea-floor sediment on its own. But, for relatively weak, water-rich sediments, entrainment is enhanced by strong high-frequency vertical motions ($PGA = 1g$) (Figs. 3 and 5). Our experiments do not include high-frequency shear wave motions, which might also contribute to remobilizing sediment.

Acknowledgements

This work was funded by National Science Foundation OCE-2044915. We would like to acknowledge the support of Erik Steen, Chris Milliren and Erik Noren in the development of the experiment, and John Leeman from Leeman Geophysical for the construction of the shaking table.

Data availability

The data used for this manuscript are the recording videos of each run. Reduced-resolution copies of the videos are available at the following archival identifier: <https://hdl.handle.net/11299/263944>.

Competing interests

The authors declare that they have no conflict of interest.

References

- Arai, K., Naruse, H., Miura, R., Kawamura, K., Hino, R., Ito, Y., ... & Kasaya, T. (2013). Tsunami-generated turbidity current of the 2011 Tohoku-Oki earthquake. *Geology*, 41(11), 1195-1198.
- Ashi, J., Sawada, R., Omura, A., & Ikehara, K. (2014). Accumulation of an earthquake-induced extremely turbid layer in a terminal basin of the Nankai accretionary prism. *Earth, Planets and Space*, 66(1), 1-9.



- Escobar, M. T., Takahata, N., Kagoshima, T., Shirai, K., Tanaka, K., Park, J.-O., et al. (2019). Assessment of Helium Isotopes
 205 Near the Japan Trench 5 Years after the 2011 Tohoku-Oki Earthquake. *ACS Earth Space Chem.* 3, 581–
 587. doi:10.1021/acsearthspacechem.8b00190.
- Fujiwara, T., Kodaira, S., No, T., Kaiho, Y., Takahashi, N., & Kaneda, Y. (2011). The 2011 Tohoku-Oki earthquake:
 Displacement reaching the trench axis. *Science*, 334(6060), 1240-1240.
- Goldfinger, C., Nelson, C. H., Johnson, J. E., & Shipboard Scientific Party. (2003). Holocene earthquake records from the
 210 Cascadia subduction zone and northern San Andreas fault based on precise dating of offshore turbidites. *Annual Review of
 Earth and Planetary Sciences*, 31(1), 555-577.
- Goldfinger, C., Nelson, C.H., Morey, A., Johnson, J.E., Gutierrez-Pastor, J., Eriksson, A.T., arabanov, E., Patton, J., Gracia,
 E., Enkin, R., Dallimore, A., Dunhill, G., Vallier, T., (2012). Turbidite Event History: Methods and Implications for Holocene
 Paleoseismicity of the Cascadia Subduction Zone. USGS Professional Paper 1661-F. U.S. Geological Survey, Reston, VA, p.
 215 184, 64
- Goldfinger, C., Ikeda, Y., Yeats, R. S., & Ren, J. (2013). Superquakes and supercycles. *Seismological Research Letters*, 84(1),
 24-32.
- Gomberg, J. (2018). Cascadia onshore-offshore site response, submarine sediment mobilization, and earthquake
 recurrence. *Journal of Geophysical Research: Solid Earth*, 123(2), 1381-1404.
- 220 Howarth, J. D., Orpin, A. R., Kaneko, Y., Strachan, L. J., Nodder, S. D., Mountjoy, J. J., ... & Çağatay, M. N. (2021).
 Calibrating the marine turbidite palaeoseismometer using the 2016 Kaikōura earthquake. *Nature Geoscience*, 14(3), 161-167.
- Ikehara, K., Irino, T., Usami, K., Jenkins, R., Omura, A., & Ashi, J. (2014). Possible submarine tsunami deposits on the outer
 shelf of Sendai Bay, Japan resulting from the 2011 earthquake and tsunami off the Pacific coast of Tohoku. *Marine
 Geology*, 358, 120-127.
- 225 Ikehara, K., Kanamatsu, T., Nagahashi, Y., Strasser, M., Fink, H., Usami, K., ... & Wefer, G. (2016). Documenting large
 earthquakes similar to the 2011 Tohoku-oki earthquake from sediments deposited in the Japan Trench over the past 1500
 years. *Earth and Planetary Science Letters*, 445, 48-56.
- Kodaira, S., No, T., Nakamura, Y., Fujiwara, T., Kaiho, Y., Miura, S., ... & Taira, A. (2012). Coseismic fault rupture at the
 trench axis during the 2011 Tohoku-oki earthquake. *Nature Geoscience*, 5(9), 646-650.
- 230 Kodaira, S., Nakamura, Y., Yamamoto, Y., Obana, K., Fujie, G., No, T., ... & Miura, S. (2017). Depth-varying structural
 characters in the rupture zone of the 2011 Tohoku-oki earthquake. *Geosphere*, 13(5), 1408-1424.
- Kodaira, S., Fujiwara, T., Fujie, G., Nakamura, Y., & Kanamatsu, T. (2020). Large coseismic slip to the trench during the
 2011 Tohoku-Oki earthquake. *Annual Review of Earth and Planetary Sciences*, 48, 321-343.
- Lay, T., & Bilek, S. (2007). Anomalous earthquake ruptures at shallow depths on subduction zone megathrusts. In *The
 235 seismogenic zone of subduction thrust faults* (pp. 476-511). Columbia University Press.
- Lay, T., Ammon, C. J., Kanamori, H., Xue, L., & Kim, M. J. (2011a). Possible large near-trench slip during the 2011 M w 9.0
 off the Pacific coast of Tohoku Earthquake. *Earth, planets and space*, 63, 687-692.



- Lay, T., Ammon, C. J., Kanamori, H., Yamazaki, Y., Cheung, K. F., & Hutko, A. R. (2011b). The 25 October 2010 Mentawai tsunami earthquake (Mw 7.8) and the tsunami hazard presented by shallow megathrust ruptures. *Geophysical Research Letters*, 38(6).
- Lay, T., Kanamori, H., Ammon, C. J., Koper, K. D., Hutko, A. R., Ye, L., ... & Rushing, T. M. (2012). Depth-varying rupture properties of subduction zone megathrust faults. *Journal of Geophysical Research: Solid Earth*, 117(B4).
- Lay, T. (2015). The surge of great earthquakes from 2004 to 2014. *Earth and Planetary Science Letters*, 409, 133-146.
- McHugh, C. M., Kanamatsu, T., Seeber, L., Bopp, R., Cormier, M. H., & Usami, K. (2016). Remobilization of surficial slope sediment triggered by the AD 2011 Mw 9 Tohoku-Oki earthquake and tsunami along the Japan Trench. *Geology*, 44(5), 391-394.
- McHugh, C. M., Seeber, L., Rasbury, T., Strasser, M., Kioka, A., Kanamatsu, T., ... & Usami, K. (2020). Isotopic and sedimentary signature of megathrust ruptures along the Japan subduction margin. *Marine Geology*, 428, 106283.
- Moernaut, J., Van Daele, M., Strasser, M., Clare, M. A., Heirman, K., Viel, M., ... & De Batist, M. (2017). Lacustrine turbidites produced by surficial slope sediment remobilization: a mechanism for continuous and sensitive turbidite paleoseismic records. *Marine Geology*, 384, 159-176.
- Molenaar, A., Moernaut J., Wiemer G., Dubois N., and Strasser M. (2019). Earthquake impact on active margins: tracing surficial remobilization and seismic strengthening in a slope sedimentary sequence. *Geophysical Research Letters* 46, no. 11: 6015-6023
- Molenaar A., Van Daele M., Vandorpe T., Degenhart G., De Batist M., Urrutia R., Pino M., Strasser M., and Moernaut J. (2021). What controls the remobilization and deformation of surficial sediment by seismic shaking? Linking lacustrine slope stratigraphy to great earthquakes in South-Central Chile. *Sedimentology* 68, no. 6: 2365-2396.
- Nakamura, T., Takenaka, H., Okamoto, T., Ohori, M., & Tsuboi, S. (2015). Long-period ocean-bottom motions in the source areas of large subduction earthquakes. *Scientific reports*, 5(1), 16648.
- Noguchi, T., Tanikawa, W., Hirose, T., Lin, W., Kawagucci, S., Yoshida-Takashima, Y., ... & Okamura, K. (2012). Dynamic process of turbidity generation triggered by the 2011 Tohoku-Oki earthquake. *Geochemistry, Geophysics, Geosystems*, 13(11).
- Oguri, K., Kawamura, K., Sakaguchi, A., Toyofuku, T., Kasaya, T., Murayama, M., ... & Kitazato, H. (2013). Hadal disturbance in the Japan Trench induced by the 2011 Tohoku-Oki Earthquake. *Scientific Reports*, 3(1), 1915.
- Pouderoux, H., Proust, J. N., & Lamarche, G. (2014). Submarine paleoseismology of the northern Hikurangi subduction margin of New Zealand as deduced from Turbidite record since 16 ka. *Quaternary Science Reviews*, 84, 116-131.
- Ratzov, G., Cattaneo, A., Babonneau, N., Déverchère, J., Yelles, K., Bracene, R., Courboux, F. (2015) Holocene turbidites record earthquake supercycles at a slow-rate plate boundary. *Geology*; 43 (4): 331–334. doi: <https://doi.org/10.1130/G36170.1>
- Seibert, C., Feuillet, N., Ratzov, G., Beck, C., Morena, P., Johannes, L., ... & Woerther, P. (2024). Sedimentary Records in the Lesser Antilles Fore-Arc Basins Provide Evidence of Large Late Quaternary Megathrust Earthquakes. *Geochemistry, Geophysics, Geosystems*, 25(2), e2023GC011152.



- Strasser, M., Kölling, M., Ferreira, C. D. S., Fink, H. G., Fujiwara, T., Henkel, S., ... & JAMSTEC Cruise MR12-E01 scientists. (2013). A slump in the trench: Tracking the impact of the 2011 Tohoku-Oki earthquake. *Geology*, 41(8), 935-938.
- Tamura, T., Sawai, Y., Ikehara, K., Nakashima, R., Hara, J., & Kanai, Y. (2015). Shallow-marine deposits associated with the 2011 Tohoku-oki tsunami in Sendai Bay, Japan. *Journal of Quaternary Science*, 30(4), 293-297.
- 275 Toyofuku, T., Duros, P., Fontanier, C., Mamo, B., Bichon, S., Buscail, R., ... & Kitazato, H. (2014). Unexpected biotic resilience on the Japanese seafloor caused by the 2011 Tōhoku-Oki tsunami. *Scientific Reports*, 4(1), 7517.
- Usami, K., Ikehara, K., Jenkins, R. G., & Ashi, J. (2017). Benthic foraminiferal evidence of deep-sea sediment transport by the 2011 Tohoku-oki earthquake and tsunami. *Marine Geology*, 384, 214-224.
- Usami, K., Ikehara, K., Kanamatsu, T., & McHugh, C. M. (2018). Supercycle in great earthquake recurrence along the Japan
 280 Trench over the last 4000 years. *Geoscience Letters*, 5(1), 1-12.
- Van Daele, M., Araya-Cornejo, C., Pille, T., Vanneste, K., Moernaut, J., Schmidt, S., ... & Cisternas, M. (2019). Distinguishing intraplate from megathrust earthquakes using lacustrine turbidites. *Geology*, 47(2), 127-130.
- Von Huene, R., Klaeschen, D., Cropp, B., & Miller, J. (1994). Tectonic structure across the accretionary and erosional parts of the Japan Trench margin. *Journal of Geophysical Research: Solid Earth*, 99(B11), 22349-22361.
- 285 Yue, H., & Lay, T. (2011). Inversion of high-rate (1 sps) GPS data for rupture process of the 11 March 2011 Tohoku earthquake (Mw 9.1). *Geophysical Research Letters*, 38(7).
- Yue, H., & Lay, T. (2013). Source rupture models for the M w 9.0 2011 Tohoku earthquake from joint inversions of high-rate geodetic and seismic data. *Bulletin of the Seismological Society of America*, 103(2B), 1242-1255